Boron diffusion in magnetic tunnel junctions with MgO (001) barriers and CoFeB electrodes

H. Kurt,[1,a] K. Rode,[1] K. Oguz,[1] M. Boese,[2] C. C. Faulkner,[2] and J. M. D. Coey[1]
[1]*School of Physics and CRANN, Trinity College, Dublin 2, Ireland*
[2]*Advanced Microscopy Laboratory, CRANN, Trinity College, Dublin 2, Ireland*

(Received 28 May 2010; accepted 4 June 2010; published online 28 June 2010)

Boron diffusion out of the CoFeB layers in model systems with thick CoFeB and MgO layers grown by radiofrequency sputtering or electron-beam evaporation and in MgO-based magnetic tunnel junctions (MTJs) is probed after annealing by x-ray photoemission spectroscopy (XPS) and electron energy loss spectroscopy. Successive interfaces are exposed by ion milling the stacks, layer by layer, in the XPS system. Despite the presence of thick CoFeB and a high annealing temperature of 400 °C, we found no boron in the MgO or at the MgO/CoFe interfaces. Similar results are also obtained in the MTJs. © *2010 American Institute of Physics*. [doi:10.1063/1.3457475]

MgO (001) barrier based magnetic tunnel junctions (MTJs) with giant tunneling magnetoresistance (TMR) have attracted a lot of interest due to their potential for magnetic sensors with high signal to noise ratios. They are also valuable for high speed nonvolatile memory elements[1,2] and high power microwave sources[3] driven by spin transfer torque. The fabrication of these junctions is not straightforward and extensive research is ongoing on the optimization of the stack in order to improve the TMR and the signal-to-noise ratio. The simplest reliable way to make these junctions involves the use of boron-containing amorphous ferromagnetic electrodes such as $Co_{40}Fe_{40}B_{20}$, which are subsequently crystallized in a bcc phase using the adjacent MgO (001) barrier as a template. This requires annealing at 350–400 °C, which induces diffusion of boron atoms out of the CoFe matrix to allow crystallization of bcc CoFe.[4] Record TMR ratios above 600% at room temperature have been achieved by using thick CoFeB to suppress Ta diffusion into the MgO barrier.[5] High resolution transmission electron microscopy (HR-TEM) studies and electron energy loss spectroscopy (EELS) of high quality MgO barriers have shown no apparent formation of any secondary phase in the annealed MTJs, although there is diffusion of Ta, B, and Mn at the atomic level.[5,6] However, recent reports from Cornell group[7,8] show that boron diffuses toward the MgO barrier on annealing, forming an Mg–B–O composite at the interface between MgO and CoFe. When MgO is thin, an Mg–B–O barrier is formed. Manganese also diffuses toward MgO from the IrMn layer used for exchange bias. High TMR ratios up to 200% at room temperature with low resistance area product were observed[8] despite the formation of Mg–B–O barriers, contrary to the common understanding that a high-quality crystalline MgO barrier is a prerequisite for high TMR.

Recently, we demonstrated high TMR ratios in junctions with electron beam (EB) evaporated MgO barriers and CoFeB electrodes.[9] These devices exhibit significantly lower noise compared to junctions made with radio frequency (rf) sputtered barriers.[10] Here we investigate boron migration on annealing junctions with CoFeB electrodes and thick (10 nm) or thin (2.5 nm) MgO barriers fabricated using conventional rf sputtering or EB evaporation. We use both x-ray photoemission (XPS) and EELS to probe the barriers and find that boron always diffuses away from the crystalline MgO barrier.

To study the crystallization process and boron diffusion, three different model samples were grown on Si/SiO_x substrates as follows (all thicknesses in nanometer):

(1) CoFeB(60)/MgO(10)/CoFeB(20).
(2) Ta(10)/CoFeB(60)/MgO(10)/CoFeB(20).
(3) Ta(10)/CoFeB(60)/MgO(10)/CoFeB(20)/Ta(10).

Each sample was made with both rf-sputtered and EB-evaporated MgO. All metallic layers were dc-magnetron sputtered at ambient temperature. CoFeB films were sputtered from a 3N purity stoichiometric $Co_{40}Fe_{40}B_{20}$ (at. %) target. MgO films were deposited using 4N purity sintered targets. Detailed deposition conditions can be found in Ref. 9. To ensure there is no shortage of boron in the system, we used thick CoFeB layers. All samples were annealed at 400 °C for 1 h. After annealing, 2θ-θ scans were performed using Cu $K\alpha_1$ radiation to determine the crystallinity of the MgO barrier as well as the crystallization of CoFe. We observed clear crystallization of bcc CoFe (001). The positions of these peaks were identical for all samples studied, indicating no major physical differences in terms of the crystallization of CoFe layers.[11] However, the corresponding CoFe lattice spacing is smaller than expected for a $Co_{50}Fe_{50}$ bcc alloy, indicating a Co-rich composition ($Co_{60}Fe_{40}$).[12] This is probably due to a slightly higher sputtering yield of Co compared to Fe. From the point of view of CoFe crystallization and boron diffusion we find no differences when a Ta cap and/or buffer layer was present. Henceforth, we focus on sample structure 1.

The *d*-spacing of the rf-sputtered MgO is slightly higher than for the EB evaporated MgO, which is exactly the same as that of bulk MgO.[9] This is also the case for the as-grown samples, where the CoFeB on both sides is amorphous and cannot induce lattice strain. Therefore we conclude that the EB-MgO is closer to the stoichiometric composition.

Upon annealing, a boron-rich surface layer was observed for samples 1 and 2 (no Ta cap layer) in x-ray reflectivity measurements. This top layer is not observed in sample 3 and we conclude that the Ta cap inhibits its observation.

[a]Electronic mail: kurth@tcd.ie.

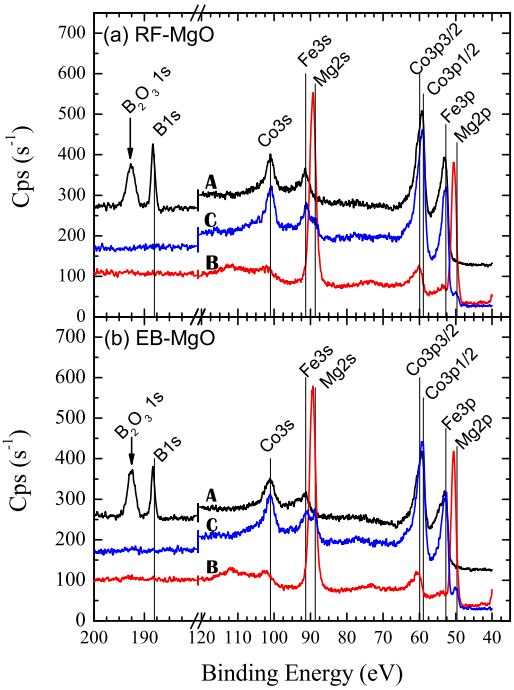

FIG. 1. (Color online) XPS surface scans of postannealed CoFeB(60)/MgO(10)/CoFeB(20) (all thicknesses are in nanometer) samples grown with (a) EB-MgO and (b) rf-MgO. Curves represent A: CoFeB(20) surface, B: MgO(10)/CoFeB(20) interface, and C: CoFeB(60)/MgO(10) interface. Intensity is offset by +100 cps for A. Note that boron is only seen at the top surface.

Compositional analysis of the sample was carried out using XPS. All measurements were carried out in normal emission mode. On the top surface of CoFeB(20) we detect B and B_2O_3 (Fig. 1). The MgO/CoFeB(20) interface, the core of the MgO layer and the CoFeB(60)/MgO interface were exposed by controlled Ar ion milling of the sample using a Hiden Analytical secondary ion mass spectrometer. Immediately after ion milling, the samples were transferred into the XPS system in air. It is therefore expected that in the first scan we observe native oxides of Fe, Co and Mg, as well as C. However, we detect neither boron nor its native oxide.

Using an Ar ion mill in the XPS system, we removed a few monolayers to expose clean interfaces for XPS. In this case, both Fe and Co peaks were detected along with the MgO but no B peak was seen. We removed the surface atoms layer by layer to expose the core of the MgO layer to the x-ray beam. Boron was absent in all cases, indicating that it *diffuses away from and not into the MgO barrier.*

To probe the bottom CoFeB/MgO interface, we continued etching down to the last few nanometer of MgO. As in the previous case, the samples were immediately loaded into the XPS chamber. We scanned the surface of these samples by removing the surface atoms layer by layer. Again we observed the same absence of boron at the bottom interface.

In order to confirm this result, we prepared TEM lamellae with a thickness adapted to EELS analysis. While the sensitivity of EELS to impurities is much higher than that of XPS, it probes a very small volume, and may therefore miss impurities if their distribution is inhomogeneous. Figure 2 shows line scans on thick rf and EB-MgO samples collected using a Gatan Tridiem 863 EELS detector. We observe no boron within the thick MgO, or at its interface with CoFe. Representative HR-TEM images are shown in Figs. 2(c) and 2(d) for EB and rf-MgO samples, which reveal high quality (001) ordering and CoFe crystallization upon annealing. We also checked the samples on a wider scale (not shown) and observed high density defect-free MgO without clustering of any other species. HR-TEM images also show a more strained CoFe/EB-MgO interface compared to the CoFe/rf-MgO. The higher *d*-spacing of rf-MgO most likely implies a tetragonal distortion with reduced in-plane lattice spacing, thereby matching better with the CoFe.

We now turn to results on MTJs with 2.5 nm thick MgO barriers, which show 240%–300% TMR at room temperature. The MTJ stacks comprise Si/SiO_x substrate/Ta 5/Ru 30/Ta 5/NiFe 5/IrMn 10/CoFe 2.5/Ru 0.9/CoFeB 3/MgO 2.5/CoFeB 3/Ta 5 and the MgO is deposited by rf sputtering or EB-evaporation. Using the same sample preparation method for XPS, we uncovered the CoFe/MgO interfaces and the MgO barrier. In normal emission the depth probed can be estimated from the electron free mean path. Using data from the universal curve, the electron escape depth is ~3 nm. Figure 3 shows the relative intensities of the species that are detected after removal of each layer. At first we observe high intensities of Ta and B together with CoFe. As we remove layers, the CoFe and Mg intensities increase and B intensity decreases. When the Mg intensity reaches its maximum there is no B. At this maximum Mg intensity we still detect the photoelectrons from Co and Fe, due to their close proximity to the surface. This holds for both types of MgO barriers, showing that boron migrates away from the MgO and into the layer on the other side of the CoFeB. If there are any boron atoms bound to the oxygen dangling bonds at the MgO surface,[13] we do not detect them due to their very low concentration in our samples.

Diffusion in alloys and/or layered structures is usually favored if the ionic radius of one of the species is much smaller than that of another with which it is in contact. Heating speeds up the diffusion when the species are mutually

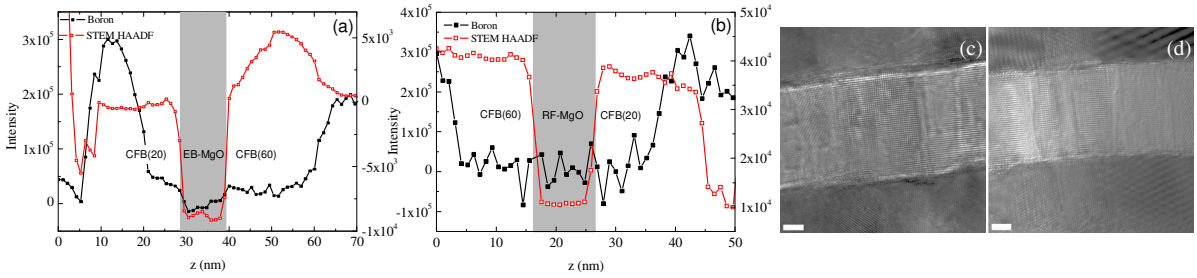

FIG. 2. (Color online) EELS scans and HR-TEM micrographs on 10 nm thick [(a) and (c)] EB-MgO and [(b) and (d)] rf-MgO annealed at 400 °C for 1 h. Scale bars are 2 nm.

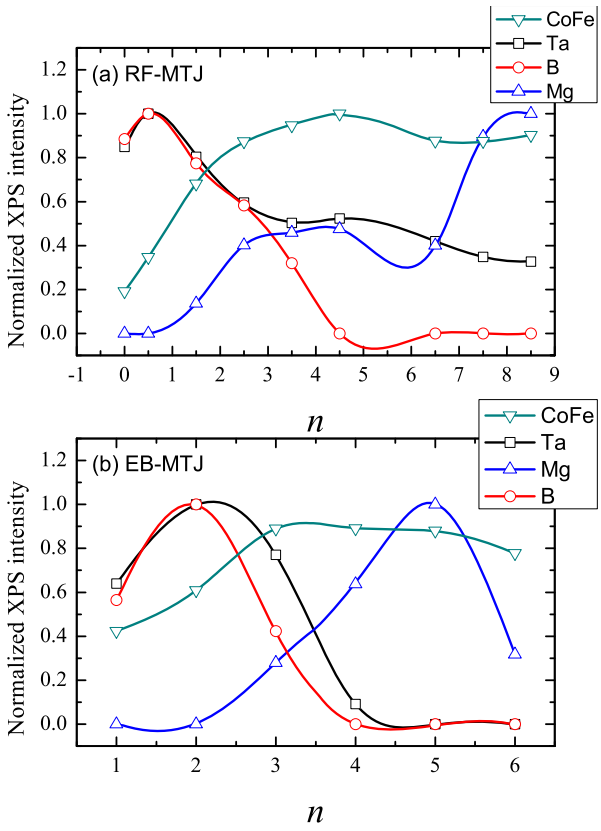

FIG. 3. (Color online) Normalized XPS intensities of CoFe (down triangle), Ta (square), Mg (up triangle), and B (circle) in (a) rf-MTJ and (b) EB-MTJ vs number of etching cycles, n, in XPS system.

soluble. While B^+ and B^{3+} cations have smaller ionic radii, Fe^{2+} and Co^{2+} cations have larger ionic radii with respect to Mg^{2+} (78 pm), which inhibits Co and Fe diffusion in MgO but suggests an easier path for B. The valence mismatch between B and Mg does not allow dissolution of B in MgO.[14] On the other hand, due to the strong affinity of B and O, a BO_x interfacial layer can form at the MgO/CoFe interface and at the grain boundaries in MgO; it has been suggested that this should degrade the TMR ratio.[13] A ternary Mg–B–O phase could form in the presence of Mg^+ states in MgO but this would require a high density of oxygen vacancies.[15]

Oxygen deficient MgO layers may absorb some boron, at the cost of lowering the barrier height.[8] An MgO barrier, which can absorb boron, could help to realize double MTJs with CoFeB middle layers. Such structures have been studied by several groups, but most attempts to fabricate double MTJs with CoFeB electrodes have failed to produce high TMR ratios due to the trapping of boron in CoFeB middle layer.[16–19] Since the amorphous middle layer cannot crystallize by losing B into the adjacent MgO barriers, coherent tunneling is not realized. In a recent study by Jiang *et al.*,[20] over 1000% TMR at room temperature is achieved by using Mg insertion layers for MgO barriers and a discontinuous CoFeB middle layer. We speculate that Mg insertion layers might have helped the crystallization of the middle CoFeB, while keeping the crystallinity of MgO. While this is a dramatic result, it has not yet been reproduced. Since the MgO barriers are grown under different conditions from different sources, it is not surprising to find different barrier characteristics from different groups.

In conclusion, we have fabricated MTJs with high TMR ratios and model junctions with thick MgO and CoFeB electrodes. Upon annealing at 400 °C, clear crystallization of bcc CoFe was observed for both rf and EB-MgO samples. XPS and EELS show no diffusion of boron into either rf or EB-MgO despite a large boron reservoir and a high annealing temperature. We find that high-quality MgO barriers do not absorb boron. On the other hand, a high density of oxygen vacancies created during MgO deposition may allow boron to diffuse in the barrier. Boron-absorbing MgO barriers could allow coherent crystallization of a middle electrode in a double MTJ but this remains to be demonstrated.

We thank Cormac McGuinness, Karsten Fleischer, and Nikolaous Peltekis for their assistance with the XPS measurements and useful discussions. This research was supported by Science Foundation Ireland (SFI) as part of the MANSE project (Contract No. SFI 05/IN/1850). It was conducted in the framework of the INSPIRE program, funded by the Irish Government's Programme for Research in Third Level Institutions, Cycle 4, 2007–2013.

[1] S. S. P. Parkin, C. Kaiser, A. Panchula, P. M. Rice, B. Hughes, M. Samant, and S.-H. Yang, Nature Mater. **3**, 862 (2004).
[2] S. Yuasa, T. Nagahama, A. Fukushima, Y. Suzuki, and K. Ando, Nature Mater. **3**, 868 (2004).
[3] A. M. Deac, A. Fukushima, H. Kubota, H. Maehara, Y. Suzuki, S. Yuasa, Y. Nagamine, K. Tsunekawa, D. D. Djayaprawira, and N. Watanabe, Nat. Phys. **4**, 803 (2008).
[4] D. D. Djayaprawira, K. Tsunekawa, M. Nagai, H. Maehara, S. Yamagata, N. Watanabe, S. Yuasa, Y. Suzuki, and K. Ando, Appl. Phys. Lett. **86**, 092502 (2005).
[5] S. Ikeda, J. Hayakawa, Y. Ashizawa, Y. M. Lee, K. Miura, H. Hasegawa, M. Tsunoda, F. Matsukura, and H. Ohno, Appl. Phys. Lett. **93**, 082508 (2008).
[6] S. V. Karthik, Y. K. Takahashi, T. Ohkubo, K. Hono, S. Ikeda, and H. Ohno, J. Appl. Phys. **106**, 023920 (2009).
[7] J. J. Cha, J. C. Read, Jr., W. F. Egelhoff, P. Y. Huang, H. W. Tseng, Y. Li, R. A. Buhrman, and D. A. Muller, Appl. Phys. Lett. **95**, 032506 (2009).
[8] J. C. Read, J. J. Cha, Jr., W. F. Egelhoff, H. W. Tseng, P. Y. Huang, Y. Li, D. A. Muller, and R. A. Buhrman, Appl. Phys. Lett. **94**, 112504 (2009).
[9] H. Kurt, K. Oguz, T. Niizeki, and J. M. D. Coey, J. Appl. Phys. **107**, 083920 (2010).
[10] Z. Diao, J. F. Feng, H. Kurt, G. Feng, and J. M. D. Coey, Appl. Phys. Lett. **96**, 202506 (2010).
[11] See supplementary material at http://dx.doi.org/10.1063/1.3457475 for 2θ x-ray diffraction data of the 400 °C postannealed CoFeB(60)/MgO(10)/CoFeB(20) samples prepared by rf and EB-MgO.
[12] M. Shiga, AIP Conf. Proc. **18**, 463 (1974).
[13] J. D. Burton, S. S. Jaswal, E. Y. Tsymbal, O. N. Mryasov, and O. G. Heinonen, Appl. Phys. Lett. **89**, 142507 (2006).
[14] C. Y. You, T. Ohkubo, Y. K. Takahashi, and K. Hono, J. Appl. Phys. **104**, 033517 (2008).
[15] S. S. Mukherjee, D. MacMahon, F. Bai, C.-L. Lee, and S. K. Kurinec, Appl. Phys. Lett. **94**, 082110 (2009).
[16] G. Feng, S. Van Dijken, and J. M. D. Coey, J. Appl. Phys. **105**, 07C926 (2009).
[17] H. D. Gan, S. Ikeda, W. Shiga, J. Hayakawa, K. Miura, H. Yamamoto, H. Hasegawa, F. Matsukura, T. Ohkubo, K. Hono, and H. Ohno, Appl. Phys. Lett. **96**, 192507 (2010).
[18] G. Feng, S. van Dijken, and J. M. D. Coey, Appl. Phys. Lett. **89**, 162501 (2006).
[19] J. M. Almeida, P. Wisniowski, and P. P. Freitas, J. Appl. Phys. **103**, 07E922 (2008).
[20] L. Jiang, H. Naganuma, M. Oogane, and Y. Ando, Appl. Phys. Express **2**, 083002 (2009).